J Appl Electrochem (2013) 43:995–1003
DOI 10.1007/s10800-013-0593-7

RESEARCH ARTICLE

Porous Co_3O_4 nanorods as superior electrode material for supercapacitors and rechargeable Li-ion batteries

S. Vijayanand · R. Kannan · H. S. Potdar · V. K. Pillai · P. A. Joy

Received: 23 May 2013 / Accepted: 13 July 2013 / Published online: 24 July 2013

Abstract Porous aggregated nanorods of Co_3O_4 with a surface area of $\sim 100\ m^2\ g^{-1}$ synthesized without using any templates or surfactants give very high specific capacitance of $\sim 780\ F\ g^{-1}$ when used as electrode in a faradaic supercapacitor, with a cycle life of more than 1,000 cycles. Further, in Li-ion batteries when used as an anode, the Co_3O_4 nanorods achieved a capacity of 1155 mA h g^{-1} in the first cycle and upon further cycling it is stabilized at 820 mA h g^{-1} for more than 25 cycles. Detailed characterization indicated the stability of the material and the improved performance is attributed to the shorter Li-insertion/desertion pathways offered by the highly porous nanostructures. The environmentally benign and easily scalable method of synthesis of the porous Co_3O_4 nanorods coupled with the superior electrode characteristics in supercapacitors and Li-ion batteries provide efficient energy storage capabilities with promising applications.

Keywords Cobalt oxide · Porous nanostructures · Supercapacitor · Li-ion battery · Electrode materials

1 Introduction

The ever-growing need for better energy conversion and storage materials demand compelling improvements in the primary energy technology sector such as batteries, fuel cells, solar cells, and supercapacitors [1, 2]. Among them, Li-ion batteries (LIB) represent one of the dominant candidates for mobile phones and portable applications due to their high energy density, modularity, and long cycle life [3]. The present generation of LIB, however, uses expensive components that will restrict the growth of LIB in the next decade, urging researchers to develop better materials that are cheaper and more efficient. Transition metal oxides are known to have, in principle, higher capacity but suffer major setbacks in the perspective of cycle life [4–6]. On the other hand, the use of carbonaceous materials, such as graphitic carbon, as the negative electrode in commercial batteries have shown reasonable cycle life despite posing severe restrictions on the maximum attainable energy density along with staging and fading of capacity that is commonly observed in these electrodes [7]. This prompted the need for immense research on alternate electrode materials, from a wide variety of compounds ranging from metal oxides and intercalation compounds of transition metals to nanostructured materials such as Si/Sn-based nanowires and hybrid materials like $LiFePO_4$ [8–12].

High power density and longer cycle life are key issues for many applications such as hybrid electric vehicles, uninterruptible power supplies and backup power sources for computer memory. Supercapacitors are ideal candidates to meet these requirements [13]. Supercapacitors generally are of two types, electric double-layer (EDL) capacitors, where non-faradic processes are the key for energy storage and pseudocapacitors or faradaic capacitors, where the redox process of the active material contributes to the capacitance. In the case of porous carbon, it has been reported that the specific capacitance/unit area for the EDL is 0.1–0.2 F m^{-2}, whereas in pseudocapacitance the same is in the range of 1–5 F m^{-2} [2]. Hence, materials with pseudocapacitive nature have gained much attention in the

S. Vijayanand · R. Kannan · H. S. Potdar · V. K. Pillai · P. A. Joy (✉)
Physical and Materials Chemistry Division, CSIR-National Chemical Laboratory, Pune 411008, India
e-mail: pa.joy@ncl.res.in

field of supercapacitors which has triggered huge interest in the development of nanostructured materials for both energy conversion and storage [1, 14, 15].

Among transition metal oxides, Co_3O_4 with selective shapes has recently been demonstrated as a promising anode material for LIB technology [16–24]. The inherent advantage of the needle-like structures obtained by a virus-mediated route is utilized for increased capacity [16]. Nanowire arrays are shown to exhibit higher capacity than broken nanowires whose capacity continuously decreases with increasing cycle [17]. Co_3O_4 nanotubes are shown to give higher capacity than nanowires and nanoparticles [18]. Similarly, needle-like nanotubes offer high storage capacity and improved cycle life [19]. The influence of shape over the capacity has been demonstrated, very recently, and it has been shown that porous materials offer higher capacity [20]. For example, capacity values as high as 1450 mA h g^{-1} has been obtained for porous nanoshells obtained by a hydrothermal method of synthesis [21]. Also, in addition to the effect of size, the importance of shape and morphology of the Co_3O_4 nanostructures on the electrochemical performance have been demonstrated by Yan et al. [22]. Co_3O_4 nanowires synthesized by hydrothermal method from cobalt ion-based coordination polymer nanowires have been shown to exhibit a high reversible capacity of 810 mA h g^{-1} [23]. Similarly, high reversible capacity up to 1240 mA h g^{-1} is reported for Co_3O_4 nanowire arrays of low surface area synthesized from cobalt hydroxy carbonate precursor by the hydrothermal method, suggesting that the electrochemical performance is associated with the structural aspects rather than the specific surface area [24].

As far as the behavior of metal oxides in supercapacitors is considered, RuO_2 has been shown to exhibit a remarkable capacitance value of 720 F g^{-1}, which is marked as a new breakthrough in the development of metal oxides-based pseudocapacitors [25]. However, its toxic nature and high cost prevent the usage of RuO_2 in practical applications. This has lead to the attention toward various transition metal oxides, such as NiO [26], MnO_2 [27], $Ni(OH)_2$ [28], Co_3O_4 [29], etc., as alternate materials for supercapacitor applications. Among these, Co_3O_4-received greater attention due to its environmental friendliness, low cost, and favorable pseudocapacitor characteristics, resulting in studies on Co_3O_4 for supercapacitor applications [29, 30]. For example, connected Co_3O_4 nanoparticles with a high surface area of 225 m^2 g^{-1} and a sharp pore-size distribution of 3–4 nm has been shown to exhibit a very high specific capacitance of 623 F g^{-1}, the highest value so far reported for Co_3O_4 [29]. Wang et al. [31] synthesized porous Co_3O_4 nanowires and nanocubes using the templates SBA–15 and KIT–6 and showed that maximum capacitance of 370 and 282 F g^{-1}, respectively, can be obtained. Similarly, Cui et al. [32] reported a capacity of 456 F g^{-1} for Co_3O_4 nanorods synthesized by a microwave-assisted template approach. Likewise, Co_3O_4 nanorods synthesized by a hydrothermal method exhibited a capacity of 280 F g^{-1} [33]. For Co_3O_4 nanosheets synthesized by hydrothermal method, a capacity of 92 F g^{-1} has been reported [34]. Using ployacrylamide, through the formation of a gel, Cao et al. [35] prepared mesoporous Co_3O_4 nanoparticles which showed a capacity of 401 F g^{-1}. Thus, Co_3O_4 seems to be a possible alternate material in place of RuO_2 if it is having the properties of well-defined morphology with sharp pore-size distribution and high surface area.

Synthesis of Co_3O_4 nanostructures, without the use of templates or surfactants, is an urgent need since it can eliminate the cost and contamination due to the surfactants, avoiding complicated process of operation and impurities in the final product, apart from the environmental impact. Among all the reported methods, synthesis of novel nanostructures from co-precipitated molecular precursors is a very convenient method, which can help to control the morphology of nanostructures of Co_3O_4 by precipitating a suitable precursor with desired morphologies. For the synthesis of Co_3O_4, cobalt hydroxy carbonate is a desirable precursor, as no toxic byproducts are liberated during its pyrolysis in air [24, 36, 37]. Orientational attachment of nanocrystalline particles can be obtained by the process of controlled aggregation [38]. In recent times, immense interest is focused on nanostructured materials with high surface area and sharp pore-size distribution to enhance the transport of ions in the electrode/electrolyte interface, which in turn reflects in the faster kinetics of the electrodes [29, 39]. Hence, designing nanostructured materials having these properties is a key factor in any electrode applications, where the transport of ions is the deciding factor of the capacity such as high power density, energy density, specific capacitance, etc.

In this paper, we report the application of porous Co_3O_4 nanorods, synthesized through orientational attachment without using any surfactant or template, in the energy storage. Very high specific capacitance value of 780 F g^{-1} has been obtained with the cycle stability of more than 1,000 cycles. Also, these porous Co_3O_4 nanorods showed improved capacity in LIB application, with the capacity value of 1155 mA h g^{-1} in the first cycle and a considerably high value of 820 mA h g^{-1} even after 25 cycles without any obvious performance degradation. The mode of Li-ion transport inside the Co_3O_4 matrix during charge–discharge (CDC) process has been investigated by using ^{7}Li NMR, XRD, and magnetic measurements of the electrodes at various stages of charging (modes of operation) in conjunction with electrochemical techniques.

2 Experimental methods

Nanostructured Co_3O_4 with rod shapes was synthesized by the method of co-precipitation using cobaltous nitrate and potassium carbonate, followed by digestion and calcination [40]. The as-dried cobalt hydroxy carbonate precursor was calcined in air at 300 °C for 5 h to obtain the oxide of cobalt. The calcined sample was used for all studies and is labeled as C300.

The calcined material was characterized using different techniques such as powder X-ray diffraction (XRD) using a Panalytical Xpert PRO X-ray diffractometer, transmission electron microscopy (TEM) using SEI, PECNAI G^2TF30 transmission electron microscope, surface area and pore-size distribution using Micromeritics NOVA 1200 (Quanta Chrome) instrument using N_2 as adsorbent, magnetic measurements using a vibrating sample magnetometer (PAR EG&G), and NMR spectra were recorded on a Bruker AV 300 spectrometer, at a spinning speed of 30 kHz. To study the supercapacitive behavior of the porous Co_3O_4 nanorods, cyclic voltammogram (CV) in alkaline medium was recorded using 6 M KOH solution as the electrolyte. Co_3O_4, Vulcan XC-72 carbon and Nafion taken in the ratio 75:20:5 were mixed together and dispersed in minimum amount of isopropyl alcohol. After ultrasonication, the slurry was drop casted on the carbon paper and dried over night at 100 °C. This served as the working electrode while Ag/AgCl and Pt foil were used as the reference and counter electrodes, respectively. The sample loading on the electrode was calculated by measuring the dry weight before and after coating. CV and impedance measurements were carried out on Autolab 30 PGSTAT and Solartron instruments, respectively. For the evaluation of Co_3O_4 as an anode material for rechargeable LIB, the material, Vulcan XC-72 carbon and Nafion taken in the ratio of 75:20:5 and made into a slurry using isopropyl alcohol. The slurry was applied on a stainless steel (SS 316) mesh by the brushing method [41–43] and it was used as the working electrode after drying. Li metal served as the counter and reference electrodes with 0.1 M $LiClO_4$ in propylene carbonate (PC) as the electrolyte. CDC experiments were carried out on a home-made galvanostatic set up using a Keithley 6514 electrometer and 2010 multimeter connected in series with a variable resistance box. All the experiments were carried out in argon atmosphere.

3 Results and discussion

Powder XRD studies on C300 (shown in Fig. 7 while comparing with other samples) showed the formation of Co_3O_4 with the spinel-type structure having cubic lattice parameter of $a = 8.083$ Å. This is in good agreement with the reported value for Co_3O_4 powder ($a = 8.084$ Å; JCPDS # 78-1970). All the peaks in the XRD pattern are broad indicating the nanocrystalline nature of the sample.

Figure 1 shows the N_2 adsorption–desorption isotherm of C300. The sample exhibits adsorption isotherm with hysteresis of type IV [44], indicating porous structure of the material. The sample shows a sharp pore size distribution, with a number of pores of size less than 15 nm (inset, Fig. 1). The average pore diameter is obtained as 15.4 nm with a total pore volume of 0.367 $cm^3\ g^{-1}$. The surface area of the Co_3O_4 nanorods is measured as 95.2 $m^2\ g^{-1}$. The large surface area is probably due to the pores of nanorods and the inter-nanorod spaces since they are aggregated into large clusters. The surface area is much larger than the reported values of 54 $m^2\ g^{-1}$ for 8–13 nm particles [45], and 87.1 $m^2\ g^{-1}$ for 10–20 nm particles [46], of Co_3O_4 prepared by the co-precipitation method using ammonium carbonate as the precipitant. Thus, the high surface area and large pore volume support the fact that the aggregated particles of Co_3O_4 have a highly porous structure. The absence of any peaks at low angles in the XRD pattern of C300 confirmed the non-ordered porous structure of the Co_3O_4 nanorods.

3.1 Application in supercapacitors

Figure 2 shows the CV of C300 measured at a scan rate of 5 mV s^{-1}, using 6 M KOH as the electrolyte. The observed reversible electrochemical behavior is ideal for pseudocapacitor applications due to contributions from both faradaic and non-faradaic processes [47]. The redox peak observed for the Co^{2+}/Co^{3+} couple may play a

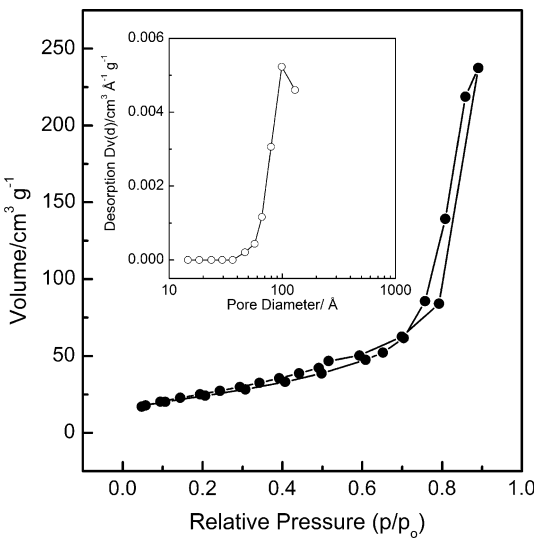

Fig. 1 Adsorption–desorption isotherms of the calcined powder C300. *Inset* pore-size distribution

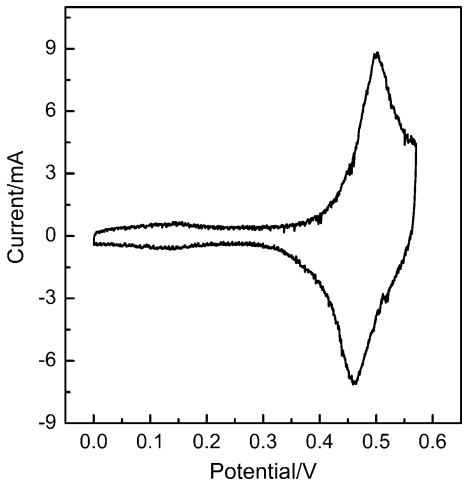

Fig. 2 Cyclic voltammogram of C300 measured at a scan rate of 5 mV s^{-1}, using 6 M KOH as the electrolyte

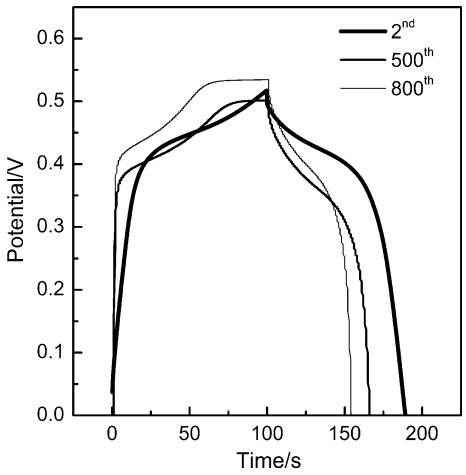

Fig. 3 Galvanostatic charge–discharge curves obtained for the sample C300 at various cycles as indicated

crucial role in improving the capacitance of the electrode. The capacitance value calculated from the CV is 780 F g^{-1} which is much higher than the reported value of 623 [29], 450 [32], and 95 F g^{-1} [34], for Co_3O_4 nanorods and micro porous nanostructures, respectively. In the present case, the large value of the specific capacitance obtained could be attributed to the enhanced surface area and higher porosity of the nanorods which improve the electrode–electrolyte interface.

To get in-depth information about the capacitive nature of the Co_3O_4 nanorod-based electrodes, CDC experiments were carried out with the charging–discharging rate equivalent to a current density of 1 A g^{-1}. The capacitance is calculated from the slope of the curve which is given by $C = I\Delta t/m\Delta V$, where I is the galvanostatic discharging current, Δt is the discharging time, ΔV is the potential drop during discharge, and m represents the mass of the electroactive material [32]. Figure 3 shows the CDC curve at different cycles. The calculated capacitance values are 776, 672, and 656 F g^{-1} for the 2nd, 500th, and 800th cycle, respectively. Also, the calculated value of 776 F g^{-1} is in close agreement with the capacitance calculated from the CV measurements (780 F g^{-1}).

The electrochemical impedance spectroscopy analysis was carried out in the frequency range of 0.01–1 MHz with ac voltage amplitude of 5 mV to further substantiate the capacitive performance of the Co_3O_4 material at the open-circuit potential (OCP). The Nyquist plots of the Co_3O_4 electrode before and after CDC are shown in Fig. 4. From the high frequency intercept at the x axis, the electrode–electrolyte total system resistance is calculated as 6.7 Ω before discharge which is reduced to 1.7 Ω after CDC experiments, revealing the increased exposure of the pores due to the prolonged operation although other parameters such as corrosion of the carbon support, etc., could have led to the observed small decrease in capacitance. This abides the fact that surface area and pore size are the key factors determining of faster electrode kinetics. Hence, the sample C300 showed a very high specific capacitance value (780 F g^{-1}).

3.2 Application as an anode material in Li-ion batteries

Figure 5 shows the CV obtained utilizing porous Co_3O_4 nanorods (C300). The CVs are measured at a scan rate of 1 mV s^{-1} over the potential window 0–3 V. The presence of two anodic peaks and one cathodic peak are observed and this may be attributed to the Li-ion insertion and desertion in the Co_3O_4 matrix. More specifically,

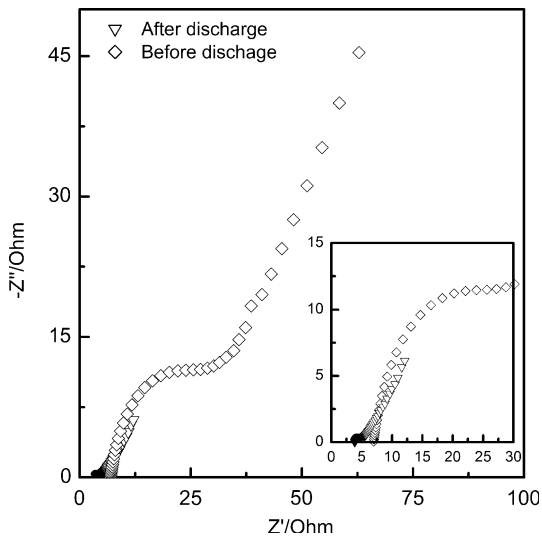

Fig. 4 Impedance Nyquist plots obtained for the sample C300 before and after charge–discharge cycles for 1,000 cycles

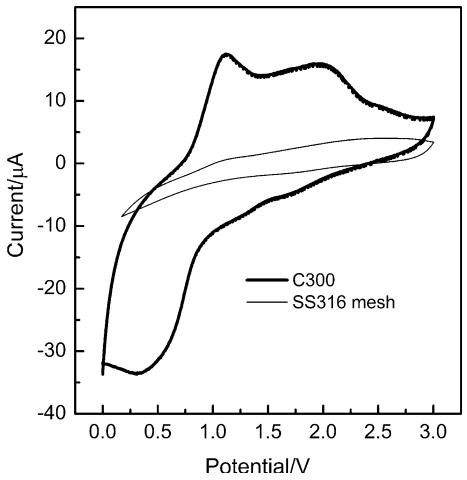

Fig. 5 CV plots measured for the C300 and bare stainless steel mesh electrodes using 0.1 M $LiClO_4$ dissolved in propylene carbonate as the electrolyte at a scan rate of 1 mV s^{-1}

the anodic peaks can be ascribed to the oxidation of Co concomitant to the intercalation of Li^+ into the Co_3O_4 matrix, whereas the cathodic peak observed at 0.7 V could be attributed to the reduction of Co_3O_4. This is in accordance with the literature reports on Co_3O_4 reduction [16, 21].

The OCP measured for the porous Co_3O_4 nanorods (C300) coupled with a Li-metal foil is 3.6 V which is in very good agreement with the reported values. Figure 6 shows the discharge capacity of the sample at the first cycle. The total capacity value of the first cycle is 1155 mA h g^{-1}. Also, the discharge capacity behavior is found to be consistent with the previous reports [18, 19, 22]. Interestingly, the cycle life measurements (inset, Fig. 6) reveal that after

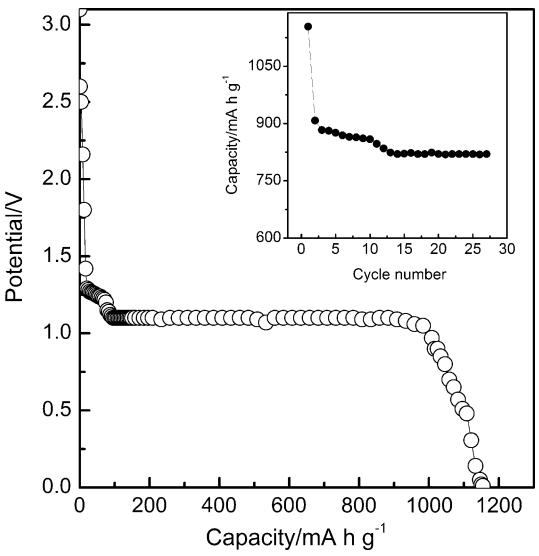

Fig. 6 Galvanostatic discharge curve of C300 at a discharge rate of 50 mA h g^{-1} using 0.1 M $LiClO_4$ dissolved in propylene carbonate. *Inset* Capacity as a function of cycle number

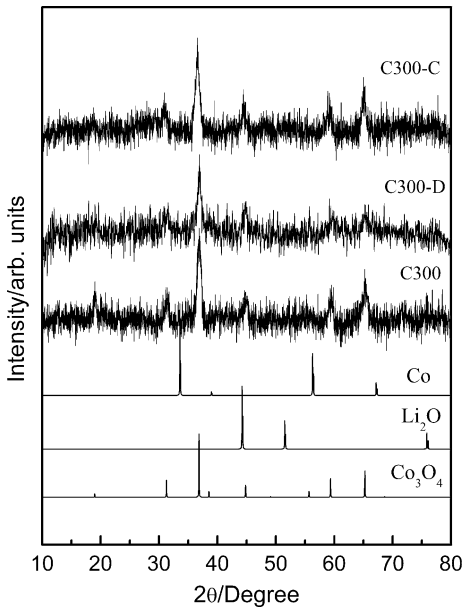

Fig. 7 Comparison of the XRD patterns of C300 (as-prepared Co_3O_4), C300-D (after complete discharging), and C300-C (after complete charging). Simulated patterns of Co, Co_3O_4 and Li_2O are shown

dropping from a capacity of 1155–908 mA h g^{-1}, the capacity of the Co_3O_4 nanorods become steady at 820 mA h g^{-1} for more than 25 cycles, which is still much higher than that of commercial carbon-based electrodes. This abides well with the fact that structures with smaller transport pathways will give better Li-insertion capabilities due to decreased volume change which is expected to give improved capacity and cycle life [15, 18]. This shows the inherent advantage of the porous, high surface area, nanorods without suffering any stress during the transportation of

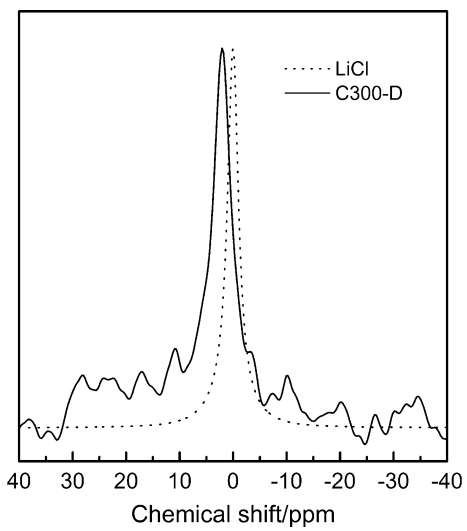

Fig. 8 ^{7}Li solid-state NMR spectra of C300-D and lithium chloride as the reference material

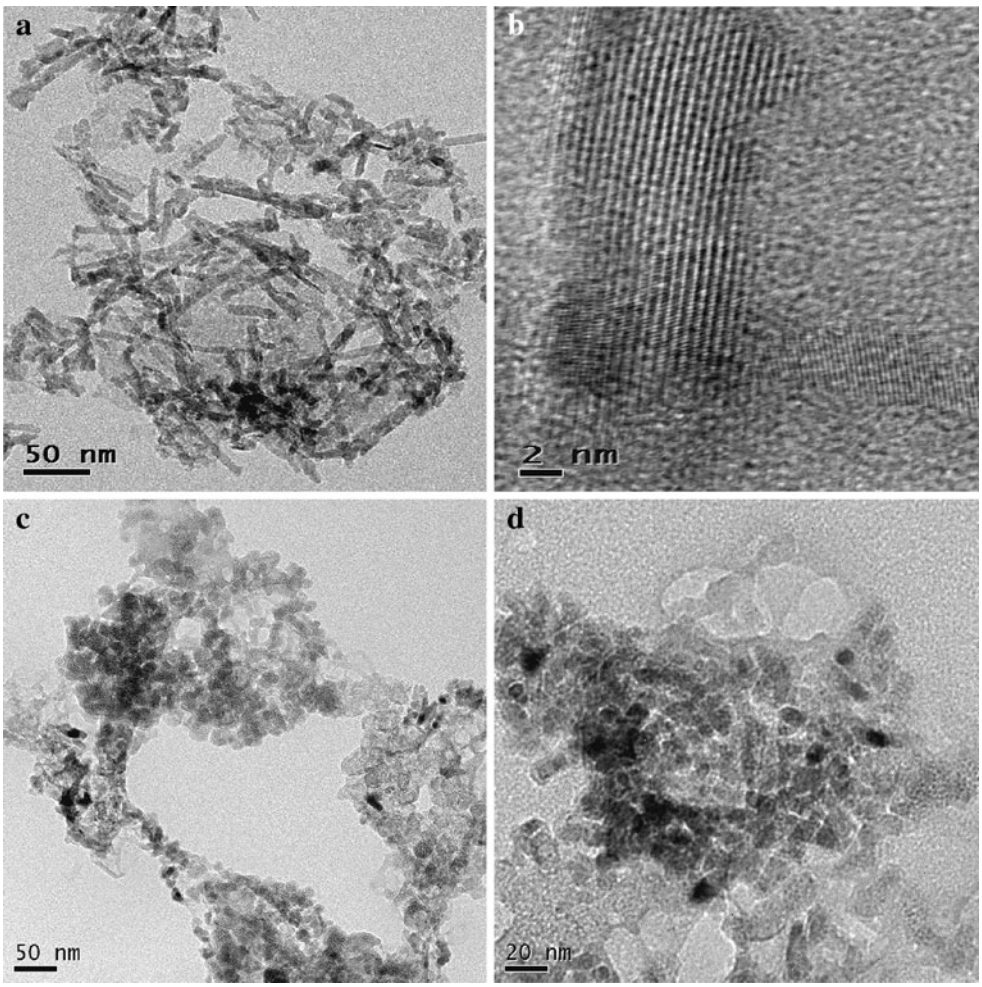

Fig. 9 TEM images of C300 (**a**, **b**), C300-C (**c**), and C300-D (**d**)

Li-ion. The capacity values are comparable to that reported for nanowire arrays with high porosity synthesized by the hydrothermal method [23, 24]. The advantage of the present material is that the highly porous nanorods are synthesized by a simple and scalable chemical approach with high surface area.

Further studies are made to understand the improved capacity of the electrode through different characterization tools like HRTEM, ^{7}Li solid-state NMR, magnetic measurements, and powder XRD. The XRD patterns recorded after charging (C300-C) and discharging (C300-D), shown in Fig. 7, do not exhibit any considerable changes when compared to that of the as-prepared Co_3O_4 (C300), demonstrating the stability of the nanorod matrix after charging and discharging. The possible operating mechanism for a metal oxide reacting with Li is the formation of nanodomains of metal and Li_2O in the metal oxide matrix during discharge and reversion of the oxide while charging back [48]. In the case of Co_3O_4 also, it is reported that there is formation of Co nanodomains with Li_2O during discharge and formation of β-CoO instead of Co_3O_4 while charging back. For example, Li et al. [17] confirmed the formation of Co metal through the observation of dark grains in the HRTEM image with the lattice fringe value corresponding to the structure of Co and the XRD pattern showed broad and weak reflections due to Li_2O and fcc Co. However, peaks due to Co and Li_2O are not observed in the XRD patterns shown in Fig. 7, indicating that probably very fine (amorphous) or nanosized Co and Li_2O are formed. Since peaks corresponding to Li_2O are not observed in the XRD pattern, changes in the Li environment during discharge was probed through ^{7}Li solid-state NMR. Figure 8 shows the ^{7}Li NMR spectra of the discharged sample where a chemical shift of 2 ppm against LiCl is observed. This result confirms the formation of Li^+ during the discharge (insertion) as the chemical shift resembles more toward Li^+ than toward metallic Li (Li^0 state) [49].

The TEM images of C300, C300-C, and C300-D are shown in Fig. 9. The pristine sample shows a well-defined rod-shaped morphological feature. Also this is clearly

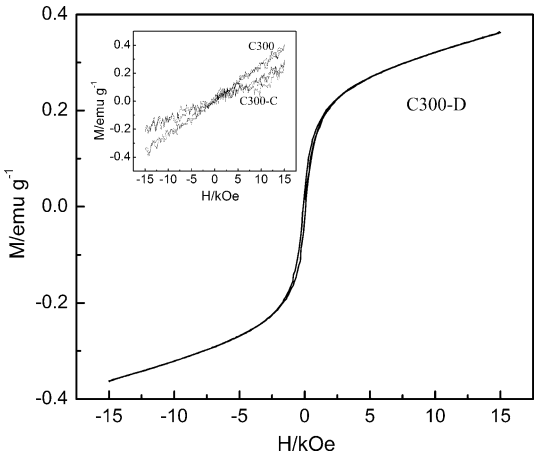

Fig. 10 Magnetic characteristics of the discharged sample (C300-D). *Inset* shows the magnetic characteristics of the pristine Co_3O_4 (C300) and the charged sample (C300-C)

evident from the lattice fringes shown. After charging (C300-C) and discharging (C300-D) back, the images are not clear perhaps due to the solvent adsorption and intercalation in the pores. Similar observation of polymeric coverage on the mesoporous nanowire arrays has been shown by Li et al. [17]. Co nanodomains were observed by Li et al. very clearly from the TEM image. The absence of peaks due to Co in XRD and fringes in HRTEM studies lead us to make use of the inherent advantage of magnetic measurements, which is an effective and sensitive tool to confirm even trace amounts of ferromagnetic Co.

Figure 10 shows the magnetization data of C300, C300-C, and C300-D (charging-discharging after ten cycles) indicating a ferromagnetic signal in the discharged sample whereas the pristine sample and the charged one do not show any ferromagnetic signal since Co_3O_4 is paramagnetic at room temperature. This confirms the formation of metallic Co in the discharged state of the material. Also, the magnetic measurements reveal that the amount of conversion of Co is very less from its magnetization value of 0.36 emu g^{-1} of the sample. For Co nanoparticles of size in the range of 10 nm, magnetization value of 20 emu g^{-1} is reported against the bulk value of 160 emu g^{-1}. This corresponds to less than 1 % of Co nanoparticles in C300-D, which proves the stability of the material. We anticipate a two-step structural modification in the Co_3O_4 matrix with initial insertion of Li leading to a modification on the Co_3O_4 matrix, which on further Li desertion regains the original structure. Even after ten CDC cycles, the material is not completely converted into metallic Co, as inferred from the XRD and magnetic measurements, which can be attributed to the stability of the material and the shorter pathways offered by the highly porous structure. Further, it could also be due to the formation of more and more active sites that would be regenerated by the redox process which is favoured here due to the structural aspects of the material.

4 Conclusions

Porous Co_3O_4 nanorods have been synthesized through a simple chemical approach without using any template or surfactant. The porous nanorods of Co_3O_4 have high surface area, high porosity, and sharp pore-size distribution. These porous nanorods are demonstrated to have a very high specific capacitance value of 780 F g^{-1} when used as an electrode material in a supercapacitor. Similarly, as an anode material, it showed a capacity of 1155 mA h g^{-1} in Li-ion battery, during initial cycles followed by excellent durability by providing 820 mA h g^{-1} for 25 cycles and beyond without any obvious signs of capacity loss or performance degradation. The enhanced capacity is due to the porous nature of the nanostructured material with high surface area, which results in reduced volume change upon Li-insertion/desertion, which also results in better cycle life. ^{7}Li solid-state NMR studies confirmed the change in Li environment during the discharge process. The XRD measurements after CDC cycles proved the stability of the material and at the same time the formation of Co nanodomains has been confirmed by magnetic measurements. The present studies show that the porous Co_3O_4 nanorods can be used as a superior electrode material for energy storage in supercapacitors as well as Li-ion batteries.

Acknowledgments Authors SV and RK are grateful to Council of Scientific and Industrial Research (CSIR), India and University Grants Commission (UGC), India, respectively, for Research Fellowships.

References

1. Arico AS, Bruce P, Scrosati B, Tarascon JM, Van Schalkwijk W (2005) Nanostructured materials for advanced energy conversion and storage devices. Nat Mater 4:366–377
2. Liu C, Li F, Ma LP, Cheng HM (2010) Advanced materials for energy storage. Adv Mater 22:E28–E62
3. Nazri G, Pistoia G (2004) Lithium batteries: science and technology. Springer, New York
4. Kang YM, Song MS, Kim JH, Kim HS, Park MS, Lee JY, Liu H, Dou S (2005) A study on the charge-discharge mechanism of Co_3O_4 as an anode for the Li ion secondary battery. Electrochim Acta 50:3667–3673
5. Park MS, Wang GX, Kang YM, Wexler D, Dou SX, Liu HK (2007) Preparation and electrochemical properties of SnO_2 nanowires for application in lithium-ion batteries. Angew Chem Int Ed 46:750–753
6. Li W, Cheng F, Tao Z, Chen J (2006) Vapor-transportation preparation and reversible lithium intercalation/deintercalation of α-MoO_3 microrods. J Phys Chem B 110:119–124
7. Yoon SH, Park CW, Yang HJ, Korai Y, Mochida I, Baker RTK, Rodriguez NM (2004) Novel carbon nanofibers of high

graphitization as anodic materials for lithium ion secondary batteries. Carbon 42:21–32
8. Chan CK, Peng HL, Liu G, McIlwrath K, Zhang XF, Huggins RA, Cui Y (2008) High-performance lithium battery anodes using silicon nanowires. Nat Nanotechnol 3:31–35
9. Gao XP, Bao JL, Pan GL, Zhu HY, Huang PX, Wu F, Song DY (2004) Preparation and electrochemical performance of polycrystalline and single crystalline CuO nanorods as anode materials for Li ion battery. J Phys Chem B 108:5547–5551
10. Wang Y, Zeng HC, Lee JY (2006) Highly reversible lithium storage in porous SnO_2 nanotubes with coaxially grown carbon nanotube overlayers. Adv Mater 18:645–649
11. Kim DW, Hwang IS, Kwon SJ, Kang HY, Park KS, Choi YJ, Choi KJ, Park JG (2007) Highly conductive coaxial SnO_2–In_2O_3 heterostructured nanowires for Li ion battery electrodes. Nano Lett 7:3041–3045
12. Whittingham MS (2004) Lithium batteries and cathode materials. Chem Rev 104:4271–4301
13. Conway BE (1999) Electrochemical supercapacitors: scientific fundamentals and technological applications. Springer, New York
14. Goodenough JB, Kim Y (2010) Challenges for rechargeable Li batteries. Chem Mater 22:587–603
15. Guo YG, Hu JS, Wan LJ (2008) Nanostructured materials for electrochemical energy conversion and storage devices. Adv Mater 20:2878–2887
16. Nam KT, Kim DW, Yoo PJ, Chiang CY, Meethong N, Hammond PT, Chiang YM, Belcher AM (2006) Virus-enabled synthesis and assembly of nanowires for lithium ion battery electrodes. Science 312:885–888
17. Li Y, Tan B, Wu Y (2008) Mesoporous Co_3O_4 nanowire arrays for lithium ion batteries with high capacity and rate capability. Nano Lett 8:265–270
18. Li WY, Xu LN, Chen J (2005) Co_3O_4 nanomaterials in lithium-ion batteries and gas sensors. Adv Funct Mater 15:851–857
19. Lou XW, Deng D, Lee JY, Feng J, Archer LA (2008) Self-supported formation of needlelike Co_3O_4 nanotubes and their application as lithium-ion battery electrodes. Adv Mater 20:258–262
20. Guo B, Li C, Yuan ZY (2010) Nanostructured Co_3O_4 materials: synthesis, characterization, and electrochemical behaviors as anode reactants in rechargeable lithium ion batteries. J Phys Chem C 114:12805–12817
21. Zhan F, Geng B, Guo Y (2009) Porous Co_3O_4 nanosheets with extraordinarily high discharge capacity for lithium batteries. Chem Eur J 15:6169–6174
22. Yan N, Hu L, Li Y, Wang Y, Zhong H, Hu X, Kong X, Chen Q (2012) Co_3O_4 nanocages for high-performance anode material in lithium-ion batteries. J Phys Chem C 116:7227–7235
23. Li CC, Yin X, Chen L, Li Q, Wang T (2010) Synthesis of cobalt ion-based coordination polymer nanowires and their conversion into porous Co_3O_4 nanowires with good lithium storage properties. Chem Eur J 16:5215–5221
24. Xiong S, Chen JS, Lou XW, Zeng HC (2012) Mesoporous Co_3O_4 and CoO@C topotactically tranformed from chrysanthemum-like $Co(CO_3)_{0.5}(OH)_{0.11}H_2O$ and their lithium-storage properties. Adv Funct Mater 22:861–871
25. Zheng J, Cygan P, Jow T (1995) Hydrous ruthenium oxide as an electrode material for electrochemical capacitors. J Electrochem Soc 142:2699–2703
26. Wang Y, Xia Y (2006) Electrochemical capacitance characterization of NiO with ordered mesoporous structure synthesized by template SBA-15. Electrochim Acta 51:3223–3227
27. Rajendra Prasad K, Miura N (2004) Electrochemically synthesized MnO_2-based mixed oxides for high performance redox supercapacitors. Electrochem Commun 6:1004–1008
28. Zhao DD, Bao SJ, Zhou WJ, Li HL (2007) Preparation of hexagonal nanoporous nickel hydroxide film and its application for electrochemical capacitor. Electrochem Commun 9:869–874
29. Wei TY, Chen CH, Chang KH, Lu SY, Hu CC (2009) Cobalt oxide aerogels of ideal supercapacitive properties prepared with an epoxide synthetic route. Chem Mater 21:3228–3233
30. Zhu T, Chen JS, Lou XW (2010) Shape-controlled synthesis of porous Co_3O_4 nanostructures for application in supercapacitors. J Mater Chem 20:7015–7020
31. Wang G, Liu H, Horvat J, Wang B, Qiao S, Park J, Ahn H (2010) Highly ordered mesoporous cobalt oxide nanostructures: synthesis, characterisation, magnetic properties, and applications for electrochemical energy devices. Chem A Eur J 16:11020–11027
32. Cui L, Li J, Zhang XG (2009) Preparation and properties of Co_3O_4 nanorods as supercapacitor material. J Appl Electrochem 39:1871–1876
33. Wang G, Shen X, Horvat J, Wang B, Liu H, Wexler D, Yao J (2009) Hydrothermal synthesis and optical, magnetic, and supercapacitance properties of nanoporous cobalt oxide nanorods. J Phys Chem C 113:4357–4361
34. Xiong SL, Yuan CZ, Zhang MF, Xi BJ, Qian YT (2009) Controllable synthesis of mesoporous Co_3O_4 nanostructures with tunable morphology for application in supercapacitors. Chem Eur J 15:5320–5326
35. Cao L, Lu M, Li HL (2005) Batteries, fuel cells, and energy conversion-preparation of mesoporous nanocrystalline Co_3O_4 and its applicability of porosity to the formation of electrochemical capacitance. J Electrochem Soc 152:A871–A875
36. Belous AG, Yanchevskii OZ, Kramarenko AV (2006) Synthesis of nanosize particles of cobalt and nickel oxides from solutions. Russ J Appl Chem 79:345–350
37. Klissurski DG, Uzunova EL (1990) Synthesis of a high-dispersity copper cobaltite from a coprecipitated hydroxycarbonate. J Mater Sci Lett 9:1255–1258
38. Penn RL, Banfield JF (1999) Morphology development and crystal growth in nanocrystalline aggregates under hydrothermal conditions: insights from titania. Geochim Cosmochim Acta 63:1549–1557
39. Lin C, Ritter JA, Popov BN (1998) Characterization of sol gel derived cobalt oxide xerogels as electrochemical capacitors. J Electrochem Soc 145:4097–4103
40. Patil D, Patil P, Subramanian V, Joy PA, Potdar HS (2010) Highly sensitive and fast responding CO sensor based on Co_3O_4 nanorods. Talanta 81:37–43
41. Jena A, Munichandraiah N, Shivashankar SA (2012) Morphology controlled growth of meso-porous Co_3O_4 nanostructures and study of their electrochemical capacitive behavior. J Electrochem Soc 159:A1682–A1689
42. Park K-W, Ahn H-J, Sung YE (2002) All-solid-state supercapacitor using a nafion polymer membrane and its hybridization with a direct methanol fuel cell. J Power Sources 109:500–506
43. Ruffo R, Wessells C, Huggins RA, Cui Y (2009) Electrochemical behavior of $LiCoO_2$ as aqueous lithium-ion battery electrodes. Electrochem Commun 11:247–249
44. Sing KSW, Everett DH, Haul RAW, Moscou L, Pierotti RA, Rouquerol J, Siemieniewska T (1985) Reporting physisorption data for gas solid systems with special reference to the determination of surface-area and porosity (Recommendations 1984). Pure Appl Chem 57:603–619
45. Wang CB, Tang CW, Gau SJ, Chien SH (2005) Effect of the surface area of cobaltic oxide on carbon monoxide oxidation. Catal Lett 101:59–63
46. Baird T, Campbell KC, Holliman PJ, Hoyle RW, Stirling D, Williams BP, Morris M (1997) Characterisation of cobalt-zinc hydroxycarbonates and their products of decomposition. J Mater Chem 7:319–330

47. Liu Y, Zhao W, Zhang X (2008) Soft template synthesis of mesoporous $Co_3O_4/RuO_2{\cdot}xH_2O$ composites for electrochemical capacitors. Electrochim Acta 53:3296–3304
48. Poizot P, Laruelle S, Grugeon S, Dupont L, Tarascon JM (2000) Nano-sized transition-metal oxides as negative-electrode materials for lithium-ion batteries. Nature 407:496–499
49. Idota Y, Kubota T, Matsufuji A, Maekawa Y, Miyasaka T (1997) Tin-based amorphous oxide: a high-capacity lithium-ion-storage material. Science 276:1395–1397